Phase behaviour, micellar structure and linear rheology of tetrablock copolymer Tetronic 908

Joan Puig-Rigall[a], *Ines Obregon-Gomez*[a], *Pablo Monreal-Pérez*[a], *Aurel Radulescu*[c], *María Blanco-Prieto*[b,e], *Cécile A. Dreiss*[*d], *Gustavo González-Gaitano*[*a]

[a] Departamento de Química, Universidad de Navarra, 31080 Pamplona, Spain
[b] Departamento de Farmacia y Tecnología Farmacéutica, Universidad de Navarra, 31080 Pamplona, Spain
[c] Jülich Center for Neutron Science, JCNS Outstation at MLZ, Forschungszentrum Jülich GmbH, Lichtenbergstraße 1, 85747 Garching, Germany
[d] School of Cancer & Pharmaceutical Sciences, King's College London, Franklin-Wilkins Building, 150 Stamford Street, London SE1 9NH, UK
[e] Instituto de Investigación Sanitaria de Navarra, IdiSNA, Irunlarrea 3, 31008, Pamplona, SAPIN

Corresponding authors: gaitano@unav.es, cecile.dreiss@kcl.ac.uk

ABSTRACT

Tetronics are X-shaped block-copolymers of polyethylene oxide and polypropylene oxide, which self-assemble into micelles and undergo a sol-gel transition; these transitions are dependent on temperature, concentration but also pH, due to the central diamine group of the tetrablock. We report the nanoscale morphologies underlying these different phases and the rheology of the systems for a very large, highly hydrophilic Tetronic: T908 through the combined use of oscillatory rheology, steady-state and time-resolved fluorescence, small-angle neutron scattering (SANS), dynamic light scattering (DLS) and Fourier transform infrared attenuated total reflectance (FTIR-ATR). At low concentrations, SANS reveal core-shell micelles of ca. 10 nm radius, presenting a dehydrated core and a highly hydrated shell (94% D_2O), with relatively small aggregation numbers ($N_{agg} \approx 13$). The micelles are notably affected by the pH, due to the protonation of the central amine spacer at acidic pH (pH ≈ 2), which shifts micellization to higher temperature, with smaller micelles than at natural pH. In the intermediate concentration regime (10 to 15%), micelles are smaller ($N_{agg} \approx 4$), and present a higher hydration of the core. In the high concentration regime, Tetronic 908 undergoes a sol-gel transition above a threshold temperature, which is fully inhibited at acidic pH. SANS data from the gel phase

reveal a BCC order of tightly packed spheres. Temperature sweeps in oscillatory rheology show a shift of the onset of gelation towards lower temperatures as concentration increases, an increase in the elastic modulus *G'* and an expansion of gel region over a larger range of temperatures. SANS and rheology reveal that at slightly acidic pH, below the natural pH of ca. 8, gelation is shifted to higher temperatures, but the morphology of the gels is similar.

INTRODUCTION

Poly (ethylene oxide) (PEO)/poly (propylene oxide) (PPO) block copolymers have been studied over the last decades.[1,2] The presence of PEO and PPO moieties, of a hydrophilic and hydrophobic nature, respectively, enables their self-assembly in solution, where they form mostly spherical micelles, and more elongated structures close to phase boundaries.[3–5] Temperature, concentration, molecular weight of the blocks and their configuration can be tuned to provide a wide span of properties. The synthesis, chemical analysis, aggregation and structure, foaming and surface properties, toxicology and biological activity, as well as applications of this family of block copolymers have been extensively described in a number of classic and recent reviews.[1,6,7] In addition to their use as solubilizing agents, these amphiphilic block copolymers have also been shown to overcome multidrug resistance, a major obstacle for effective cancer therapy, by inhibiting ATP-binding cassette transporters.[2,8]

The first PEO/PPO surfactants studied and most widely used are the linear PEO-PPO-PEO triblock copolymers, known as poloxamers or Pluronic®. The full characterization of these copolymers[9] and important applications have been reported, including detergency, foaming, emulsification, lubrication, cosmetics,[10,11] and their use as vehicles for drug delivery.[2,8,12–14]

More complex architectures, such as non-linear block copolymers and multiblock copolymers, have also been studied, expanding the number of accessible morphologies.[15,16] These non-linear polymer backbones can be obtained by linking PEO and PPO blocks to a central functional group, forming for instance the category of X-shaped tetrablock copolymers referred to as poloxamines or Tetronic® (BASF). Each of the four arms comprises a PPO and a PEO block, which are connected by a central ethylene diamine spacer. Different Tetronics are obtained by varying the number of PO and EO monomers, offering a wide range of hydrophilic-lipophilic balances (HLB) and molecular weights, and hence a rich phase behaviour,[17]

dependent on both temperature and pH (due to the protonation of the central diamine group,[18,19] which can also be exploited for further chemical modification to attain other properties).[20] The micellization and gelation at high concentration and temperature of some Tetronics have been reported by us[19,21–23] mainly from a structural point of view, and by other groups.[24] However, the full characterization of this attractive class of polymers is only starting to emerge, while their applications as biomaterials are expanding.[25,26]

In this work, we report for the first time the nanostructure of T908 micelles, and its gelation in the concentrated regime. Tetronic 908 is a very large and hydrophilic poloxamine (21 PO and 114 EO units per arm, HLB>24), which shows the ability to form gels, with values of the elastic modulus similar to those of other Tetronics reported to date. Its long PEO chains make it particularly attractive to impart stealth properties to nanoparticles, namely, to prolong their circulation time by suppressing opsonization, while achieving optimum stabilisation.[27,28] It has also been used as a biomaterial, for instance in scaffolds to promote the differentiation of mesenchymal stem cells into osteoblasts[25], as well as in implant for the sustained delivery of ciprofloxacin to treat osteomyelitis.[26] In addition, its structure is reminiscent of its Pluronic counterpart, F127 (triblock with a central 60 PO units, flanked by 100 EO on each side), extensively studied as a drug carrier and for its role against multidrug resistance.[2] With approximately the same block length and double the molecular weight, T908 is broadly equivalent to two F127 which would be connected in the middle; it is therefore interesting to compare and contrast the micellar structures and gelation behaviour of these two related amphiphilic copolymers. While previous SANS studies on this Tetronic have been reported in the literature, they were specifically focused on the structure of the gel phase under flow.[29–32] This is the first structural study covering the micelles from the dilute to the concentrated regime including the gel phase, through the combined use dynamic light scattering (DLS), small-angle neutron scattering (SANS), steady-state and time-resolved fluorescence, Fourier transform infrared attenuated total reflectance (FTIR-ATR) and oscillatory rheology. We explore specifically the impact of pH and temperature on micellar structure and phase behaviour, with to develop formulations responsive to these two environmental parameters. We also carefully examine the effect of switching H_2O for D_2O, (which is necessary to obtain contrast in SANS), an effect which is often overlooked in the literature.

MATERIALS AND METHODS

Materials. Tetronic 908 (hereafter, T908) was a gift from BASF, and used without further purification, with a reported composition of 21 PO and 114 EO units per arm, HLB>24 and average molecular weight of 25,000 $g \cdot mol^{-1}$. The reported pK_as for this poloxamine are 5.2 and 7.9 for pK_{a1} and pK_{a2}, respectively.[18] With the concentrations used in this work, the solutions are slightly alkaline, with typical pH values ranging from 8.0 to 10.0. The solutions were prepared either in deionized water or in D_2O (Aldrich >99.9% in D), as specified in the text. All concentrations are expressed in weight percentage.

Sol-gel diagrams. Solutions of T908 from 5 to 40% were prepared both in water and D_2O at different pH conditions, referred to as natural (above pK_{a2}), intermediate (between pK_{a1} and pK_{a2}) and acidic (below pK_{a1}). The solutions were prepared by repeated cycles of stirring and cooling (4ºC), until a homogeneous and transparent solution was obtained. For the samples at acidic and intermediate pH, a minimal volume of concentrated commercial HCl (Aldrich, 36%) or its dilution was added to a T908 solution. The solutions were then kept at 4ºC for 24 hours before observation. About 1.5 mL of each sample was placed in a rectangular glass cuvette and introduced in a thermo-controlled Peltier cell holder, where it was gradually heated up from 20 to 70ºC in 5ºC increments (0.1ºC accuracy), and the physical appearance (sol, viscous liquid or gel) noted after 5 minutes of thermal homogenization at each temperature.

Dynamic Light Scattering (DLS). The intensity particle size distributions were obtained with either a Malvern ZetaSizer Nano or a Protein Solutions DynaPro MS/X photon correlation spectrometer (wavelengths of 633 and 820 nm, respectively). The particle size distributions were calculated from the analysis of the autocorrelation function, with the software packages implemented (ZetaSizer and DynaLS 6.0), taking into account the refractive index and viscosity of the solvent, as a function of the temperature,[33,34] which was controlled with the built-in Peltier for each instrument (0.1ºC accuracy). Prior to the measurements, samples were filtered with 0.22 μm pore size Millex syringe PVDF filters into semi-micro glass cells. In some selected solutions 0.02 μm inorganic membrane filters (Anotop, Whatman®) were used.

Small-Angle Neutron Scattering (SANS) and data analysis. SANS experiments were carried out on the KWS-2 diffractometer at the Jülich Centre for Neutron Science (JCNS), Münich, Germany.[35] An incidental wavelength of 5 Å was used with detector distances of 1.7 and 7.6 m, with a collimation length of 8 m, to cover the q range from 0.008 to 0.5 $Å^{-1}$. In the standard mode a wavelength spread $\Delta\lambda/\lambda$ = 20% was used, while in the concentrated regime, a high-resolution mode was achieved by using a collimation length of 20 m in combination with the double-disc chopper and time-of-flight data acquisition for an improved wavelength spread of $\Delta\lambda/\lambda$ = 5%. All samples were measured in quartz cells (Hellma) with a path length of 2 mm using D_2O as the solvent. The samples were placed in an aluminium rack where water was recirculated from an external Julabo cryostat, ranging temperatures from 20ºC to 65ºC. This set-up enables a thermal control with up to 0.1ºC precision. Scattered intensities were corrected for detector pixel efficiency, empty cell scattering and background due to electronic noise. The data were set to absolute scale using Plexiglas as a secondary standard. The obtained macroscopic differential cross-section $d\Sigma/d\Omega$ was further corrected for the contribution from the solvent. The complete data reduction process was performed with the QtiKWS software provided by JCNS in Garching.[35]

SANS curves were fitted using SasView 3.1.2 software.[36] Scattering curves of T908 in its unimer form were fitted with a four-arm star-shape polymer model,[37] while micelles were fitted to core-shell spheres (CSS), considering a hard-sphere (HS) structure factor in the concentrated regime. Instrumental smearing of the data was also taken into account into the calculations. The size polydispersity of the micelles was fixed at 0.2 in the fits, in accordance with the polydispersity obtained by DLS experiments, assuming a log-normal size distribution. As T908 is highly hydrophilic, it is safe to assume that the micellar shell is hydrated to a great extent. The precise degree of hydration of the hydrophilic corona was estimated from the fitted value of the scattering length density (sld) of the shell, ρ_{shell}. The solvent volume fraction in the shell is related to the scattering length densities of pure EO, ρ_{EO} and ρ_{D_2O} by:

$$x_{solv(shell)} = \frac{\rho_{shell} - \rho_{EO}}{\rho_{D_2O} - \rho_{EO}} \qquad \text{Eq. 1}$$

The same applies to the solvent in the core, where the scattering length densities of pure PO, ρ_{PO} and ρ_{D_2O} are related to solvent volume fraction by:

$$x_{solv(core)} = \frac{\rho_{core} - \rho_{PO}}{\rho_{D_2O} - \rho_{PO}} \quad \text{Eq. 2}$$

Hence, the number of water molecules, n_{solv}, in the shell and in the core can be calculated from:

$$n_{solv(shell)} = x_{solv(shell)} \frac{V_{shell}}{v_{D_2O}} \quad \text{Eq. 3}$$

$$n_{solv(core)} = x_{solv(core)} \frac{V_{core}}{v_{D_2O}} \quad \text{Eq. 4}$$

where v_{D_2O} is the volume of a molecule of solvent and V_{shell} and V_{core} are those of the shell and the core, respectively. The volume of the micelle is:

$$V_m = N_{agg} v_s + n_{solv} v_{D_2O} \quad \text{Eq. 5}$$

where v_s is the volume of the surfactant, and V_m is known from the geometrical parameters deduced from the fit (core radius and shell thickness). The aggregation number, N_{agg}, can then be readily deduced from Eq. 5, as well as the number of water molecules per ethylene oxide monomer in the shell, n_{solv}/EO.

Analysis of the SANS data from the gels was carried out using the different paracrystal models implemented in the Sasview software, as described in detail in the results section.

Steady-state and time-resolved fluorescence. Emission spectra and fluorescence lifetimes of pyrene were measured with a FLS920 spectrofluorimeter (Edinburgh Instruments), in 1 cm path-length quartz cuvettes. A 450 W Xe lamp was used as the source for the steady state fluorescence experiments, by exciting at 326 nm, with 3.0 nm excitation and emission slits. The concentration of the fluorophore was approximately $1 \cdot 10^{-7}$ mol·L^{-1}. For the study of the emission decays, the measurements were performed in the Time-Correlation Single Photon Counting (TCSPC) mode, switching the continuous source to a pulsed-diode triggered with a PDL 800-D pulse generator (PicoQuant). The nominal excitation wavelength of the LED was 310 nm, with a pulse width of 6 ns, and the emission was collected at 372 nm along 200 ns (4096 channels) for 5000 counts. Fitting of the fluorescence decays to obtain the corresponding lifetimes was performed with F900 Fluorescence Spectrometer software (Edinburgh Instruments Ltd.), by deconvolution with the scattering signal of a diluted Ludox® solution. Fluorescence decays are given by:

$$I_F = A + \sum B_i \, e^{-t/\tau_i} \qquad \text{Eq. 6}$$

where A corresponds to the background, B_i is an amplitude factor related to the intrinsic quantum yield of fluorescence and concentration of the i species, and τ_i is its corresponding fluorescence lifetime.

The addition of the amphiphile quenches the fluorescence of the pyrene. This process follows the Stern-Volmer equation:

$$\frac{\tau_0}{\tau} = 1 + K_D[Q] \quad \text{and} \quad K_D = k_q \tau_0 \qquad \text{Eq. 7}$$

where τ_0 and τ are the fluorescence lifetimes of pyrene alone and in the presence of Tetronic, respectively, k_q is the molecular bimolecular quenching constant, K_D is the Stern-Volmer quenching constant, and $[Q]$ the molar concentration of the surfactant (quencher). In all fluorescence experiments, the temperature was controlled with an external LAUDA E100 recirculating bath (0.1ºC accuracy) and N_2 was bubbled for one minute prior to the measurements directly in the cell, so as to avoid the quenching effect of the oxygen.

Rheology. Temperature, frequency and strain amplitude experiments were performed on a dynamic strain-controlled rheometer ARES (TA Instruments) using a plate-plate geometry (diameter of 25 mm) with a temperature-controlling Peltier unit. After loading the samples, a thin layer of low viscosity paraffin oil was added around the edges of the plate to prevent evaporation. Temperature ramp tests were performed at a constant angular frequency of 6.28 rad·s^{-1} and 1% strain amplitude (as obtained in the linear viscoelastic region from amplitude sweeps) covering temperatures from 20 to 80 ºC, with a heating rate of 2 ºC/min. Frequency sweep measurements were performed at 50 ºC and a constant strain of 0.5%.

Infrared Spectroscopy (FTIR-ATR). FTIR spectra of concentrated solutions of T908 in water were collected using a Shimadzu IR Affinity-1S FTIR spectrometer, equipped with a thermostated Golden Gate diamond ATR accessory. The sample was placed directly on the diamond window and covered with a cap to avoid evaporation from the solution. 32 scans per spectrum were collected at intervals of 5ºC, with a resolution of 2 cm^{-1} in the temperature range 20-70ºC. The spectra were treated with Shimadzu LabSolutions IR software, applying data interpolation to more precisely determine the features of selected vibration bands upon heating.

RESULTS AND DISCUSSION

<u>The diluted regime:</u> ***Self-Aggregation and Phase Behavior of T908.*** The phase behavior of T908 in water at natural pH (non-buffered, ca. 8.8) is shown in Figure 1.

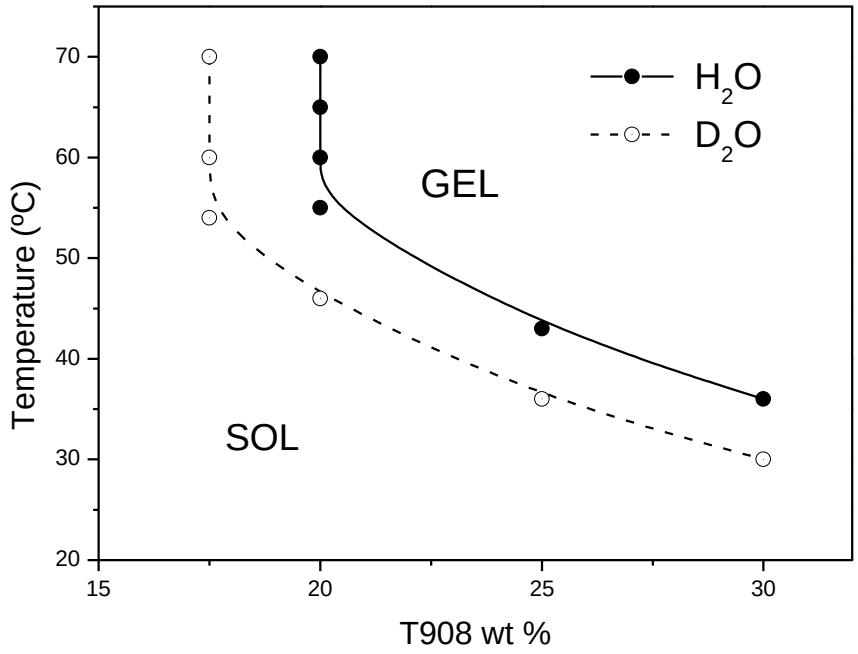

Figure 1. Phase diagram of T908 in water and D_2O showing the gel and sol regions

The threshold concentration for gel formation is 20%, when heated up to 50 ºC. At higher concentrations, the onset of gelation occurs at lower temperatures and the gel phase extends over a wider span of temperatures. At higher concentrations, the gel phase expands and at 40% the samples are gels at room temperature. At acidic pH (pH < 2, below pK_{a1}), gelation is fully suppressed at concentrations as high as 40%, and up to 70 ºC. This effect results from the protonation of the central diamine group that hinders self-assembly. A similar behaviour has been observed with Tetronic 1307, which presents nearly the same HLB (>24) but a lower molecular weight (18,000 $g \cdot mol^{-1}$).[21] By replacing H_2O by D_2O (used to optimize the contrast in SANS measurements), the onset of gelation shifts to lower temperatures (Figure 1). This effect has also been reported by Gille et al.[38] on Pluronic gels, and explained in terms of the different relative strength of the hydrogen bonds between EO and D_2O compared to H_2O.

Focusing on the effect of pH for 30% T908 with D_2O as the solvent, the phase behaviour at pH 6.6 (between pK_{a1} and pK_{a2}) shows a more gradual gel formation than at natural pH (i.e. a larger region of viscous solutions), with the onset of gelation shifting to higher temperatures compared to natural pH. This evidence suggests an important effect of the pH and a non-negligible impact of the solvent (H_2O vs. D_2O), which will be described in more detail later on through SANS and rheology experiments.

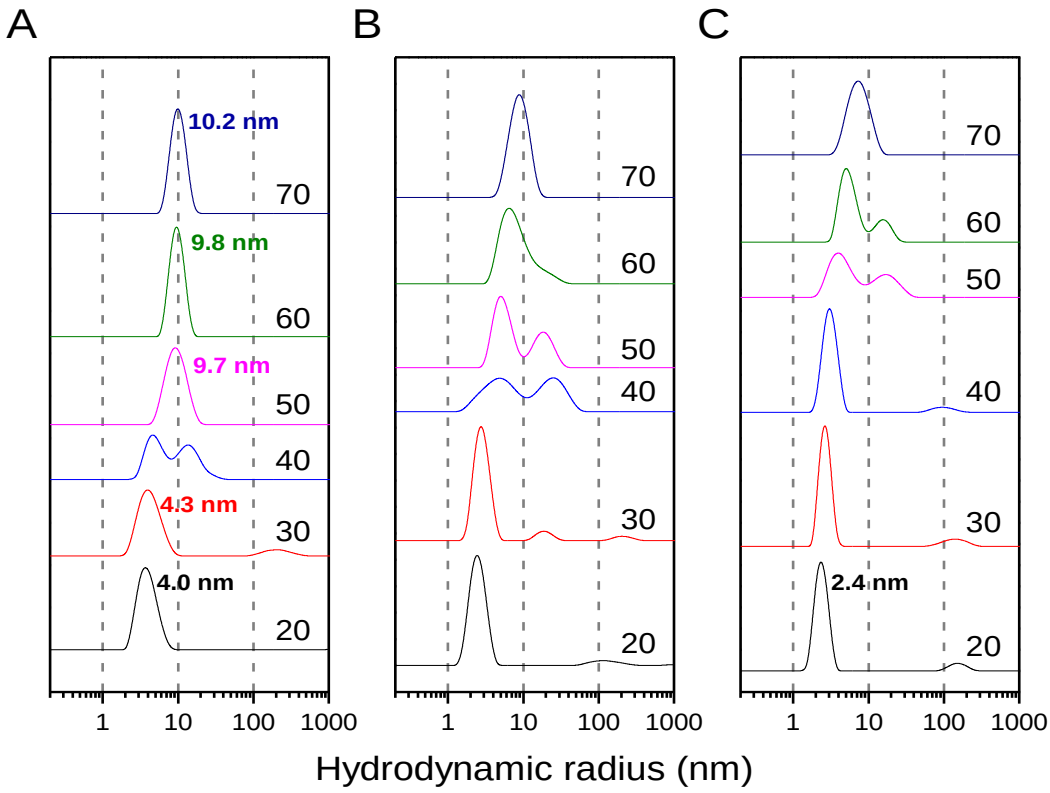

Figure 2. Intensity size distributions as a function of temperature (in ºC) obtained by DLS in D_2O: (A) 1% T908; (B) 5% T908; (C) 5% T908 buffered at pH 1.3.

In the dilute regime, both unimers and micelles are expected to coexist, above a certain temperature. Figure 2A shows the intensity size distribution in D_2O of 1% T908 at different temperatures obtained from DLS. Unimers are detected at 20 ºC, with a hydrodynamic radius, R_h, of 4.0 nm. At 30 ºC, the size distribution becomes wider and the unimers expand to 4.3 nm; at 40 ºC, the distribution becomes bimodal, marking the onset of micellization. At 50 ºC, a single peak is present with R_h = 9.7 nm, reflecting the predominance of micelles. At higher temperatures, micelles are formed, with hydrodynamic radii of 9.8 and 10.2 nm at 60 and 70 ºC, respectively, with a narrower size distribution.

To evaluate the effect of concentration on micellar size, intensity size distributions were determined at 5% T908 (Figure 2B). The general trend is similar to the one at 1% (Figure 2A): micellization also starts at 40 ºC, but the bimodal distribution (unimers + micelles) extends over a much broader range of temperatures, up to 70 ºC, suggesting a more gradual micellization, and showing a stronger impact of temperature at low concentration, in agreement with literature.[29] Acidic pH induces a shift in the micellization temperature, and a single peak corresponding to the micelles is not detected until 70 ºC (Figure 2C). The hydrodynamic radius of the unimers is very similar (R_h = 2.4 nm at 20 ºC) to the one at natural pH at the same concentration (Figure 2B). Instead, the micelles are smaller at these conditions, pointing to a lower aggregation number than at natural pH, most likely a consequence of the protonation of the diamine spacer that hinders the assembly of the PPO blocks.

More detailed structural information on the unimers and micelles in the dilute regime can be obtained from SANS. Figure 3 shows the scattering patterns obtained for T908 solutions in D_2O under different conditions. A four-arm star-shape polymer model was used to fit the scattering from the unimers, as described previously.[23,37]

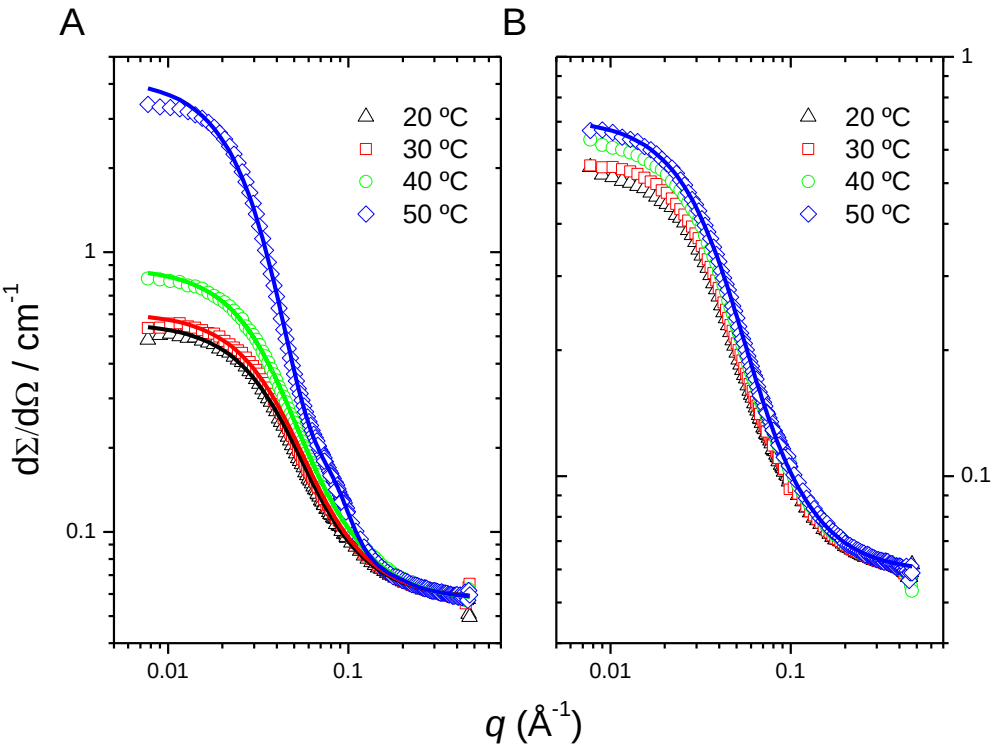

Figure 3. SANS curves for 1% T908 as a function of temperature at: (A) natural pH; and (B) pH = 2. Solid lines are fits to the different models (see text).

For 1% T908 at 20 and 30 ºC (where DLS shows that only unimers are present, Figure 2A), radii of gyration, R_g, of 4.4 and 4.5 nm are obtained (Table 1). These values are close to the hydrodynamic radii of 4.0 and 4.3 nm, respectively, obtained from DLS at the same concentration. At 40 ºC the scattering increases because of the onset of micelle formation, and at 50ºC micelles dominate the scattering (as shown also from DLS, Figure 2A), although some unimers may still be present. Hence, the overall intensity at 40 and 50 ºC can be modelled as the sum of two contributions, one due to the free unimers, and another one to the micelles, weighted by their respective volume fraction. It is reasonable to assume that, given the low concentration (1%), intermicellar interactions (and thus the structure factor) can be neglected. A core-shell sphere model (CSS) combined with a star polymer model was thus used to fit the data at these temperatures (Table 1). The radius of gyration, R_g of the unimers was set to that at 20ºC. The sld of the core consistently converged in the calculations to a small value, close to that of pure PO ($\rho_{PO} = 3.44 \cdot 10^{-7}$ Å^{-2}), reflecting a very dehydrated core, as observed for other poloxamines,[21–23] hence this parameter was also kept constant in further fits to reduce the number of fitting parameters. A simultaneous fit was performed in which the scattering length density of the shell at both 40 and 50 ºC was constrained, in order to monitor the effect on the micellar dimensions and volume fraction. The results obtained are shown in Table 1. At 50 ºC the total micellar size (core radius + shell thickness) is 9.6 nm, close to the R_h = 9.7 nm obtained by DLS (Figure 1A). The sld of the shell, ρ_{shell}, is close to that of D_2O ($6.36 \cdot 10^{-6}$ Å^{-2}), confirming the high hydration of the hydrophilic PEO corona (94% D_2O, very similar to 5% F127 micelles at 92% D_2O)[39], common in poloxamines[21,22] and poloxamers.[39,40] In comparison, F127 micelles (5%, 37 ºC) display a corona of similar thickness (6.4 nm) but a slightly larger core (4.5 nm), resulting in slightly larger micelles (ca. 10.9 nm).[39] A relatively low aggregation number is obtained with T908 (N_{agg} = 13), similar to T1107 (N_{agg} = 12)[22] and lower than T1307 (N_{agg} = 19)[21] or T904 (N_{agg} = 28)[23]. The trend indicates that the higher the hydrophilicity of the polymer, the lower the number of unimers per micelle. On the other hand, the volume fraction of micelles at 40ºC is ca. 6 times smaller than at 50ºC, suggesting that a substantial micellar phase is only obtained above 50 ºC at 1%, as also shown by DLS (Figure 2A). The micelles at this temperature are also smaller (8.2 nm), with a lower aggregation number, as they correspond to aggregates which are not yet fully formed.

Table 1. Structural parameters of 1% and 10% T908 unimers and micelles extracted from SANS data analysis at natural and acidic pH: R_g (radius of gyration of Tetronic unimers), R_c (core radius), t (shell thickness), ϕ (volume fraction), ρ_{shell} (scattering length density of the shell), N_{agg} (aggregation number), n_{solv}/EO (number of solvent molecules per EO unit in the shell).

T908 / wt%	T / ºC	R_g / Å	R_c / Å	t / Å	ϕ	$\rho_{shell} \times 10^6$ / Å^{-2}	N_{agg}	n_{solv}/EO
1	20	44	-	-	-	-	-	-
1	30	45	-	-	-	-	-	-
1	40*	44	18.2	64.2	0.002	5.81	7	93
1	50*	44	33.1	62.5	0.013	5.81	13	72
1	50 (pH = 2)	46	-	-	-	-	-	-
10	50**		37.1	54.2	0.414	6.18	5	179

*Obtained by using a combined model (star polymer + CSS)

** Obtained with a combined model (CS-HS + Ornstein-Zernicke correlation length)

The effect of acidic pH, already shown by DLS to induce a shift of the micellization to higher temperatures (Figure 2C), is also visible in the SANS curves (Figure 3B): the thermal effect on micellization is almost cancelled by acidic pH and no micellization occurs at temperatures as high as 50 ºC (only unimers of $R_g \sim 4.6$ nm are present, a size similar to natural pH).

The critical micellar concentration (*cmc*) of T908 at 25, 37 and 50 ºC was determined using pyrene fluorescence, focusing on the well-known dependence of the intensities of the I and III vibronic bands (λ_1 = 372 nm and λ_3 = 384 nm) with the micropolarity.[41] At all temperatures studied, the fluorescence of these bands (I_1 and I_3) decreases with concentration, with a marked change in the slope at 37 ºC (SI, Figure 4B) but particularly at 50 ºC (Figure 4A), while no clear tendency is detected at 25 ºC (SI, Figure 4A), in agreement with the absence of micelles at this temperature. Figure 4B represents I_1 and the I_1/I_3 ratio at 50 ºC as a function of T908 concentration. I_1 decreases with concentration due to the quenching of pyrene fluorescence produced by T908. The I_1/I_3 ratio also decreases with concentration, in accordance with the literature,[42,43] reflecting an increase in the pyrene's hydrophobic environment as the concentration of the Tetronic increases, the aggregation occurring in a rather broad interval of concentrations. The cmc can be taken as the minimum in the I_1 curve (which roughly corresponds to the inflection point of the I_1/I_3 ratio), resulting in a

value of 0.16 mM (0.4%) at 50 ºC (Figure 4B) and 0.24 mM (0.6%) at 37 ºC (SI, Figure 2B). Under different conditions (0.9% NaCl at 25 ºC), Ribeiro et al.[44] reported a cmc value of 0.24 mM , and Gonzalez-Lopez et al.[18] estimated a similar value in 10 mM HCl at 25 ºC, using surface tension measurements.

Further information about the fluorescence quenching produced by T908 on pyrene can be obtained from emission lifetime spectroscopy. The quenching effect on the pyrene decay as a function of surfactant concentration is shown in SI, Figure 3, and the decays analyzed according to Eq.6. As previously observed in the steady state experiments, the addition of the amphiphile quenches the fluorescence of pyrene, causing a faster decay (shorter lifetime) that follows Eq.7.

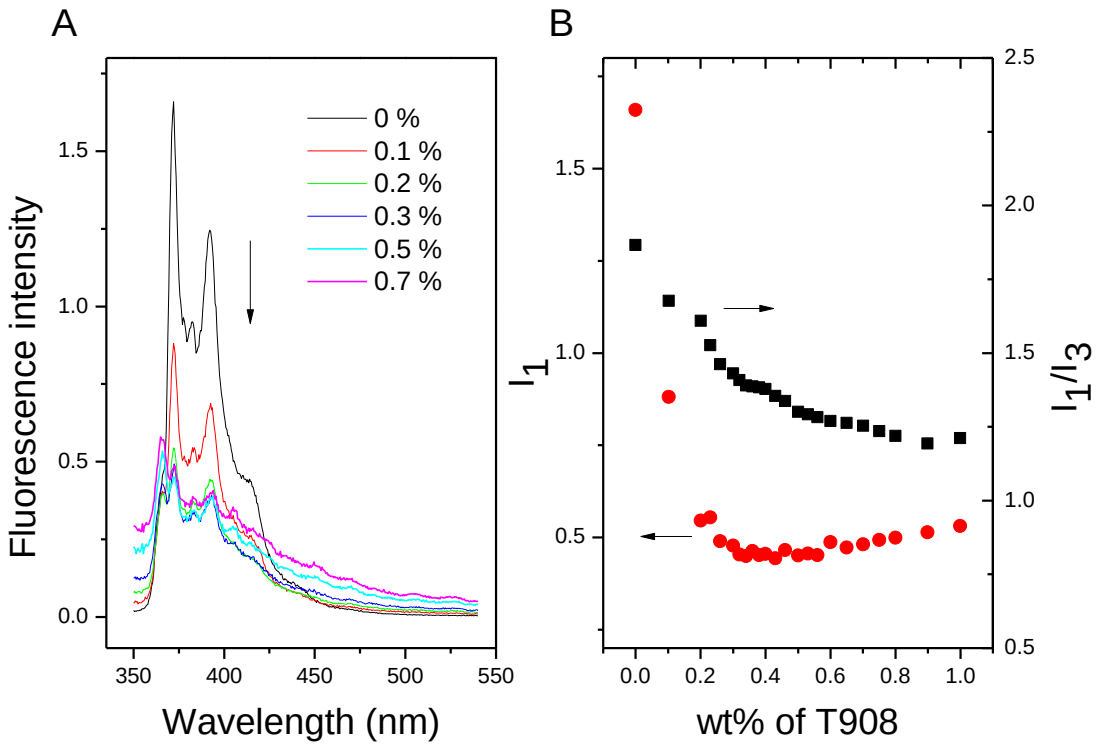

Figure 4. (A) Fluorescence spectra (arbitrary units) of pyrene as a function of the concentration of T908 at 50ºC. (B) Intensity of the I_1 vibronic band (●red) and the I_1/I_3 ratio (■black).

Pyrene lifetime has been found to depend on a number of factors, such as the nature and concentration of dissolved gasses, for example, with a typical value in water of 126 ns.[45] The presence of fluorescent impurities is usually reflected in the curves as an extra short lifetime decay whose contribution to the overall intensity is relatively small.[46] According to this, the exponential analysis done includes two decays, a slow

one for pyrene (τ_2), and a fast decay corresponding to the impurities (τ_1). The results are gathered in Table 2.

Table 2. Fluorescence lifetimes of pyrene and contributions to the overall intensity as a function of T908 concentration at 25 and 50 ºC (fluorescence lifetime of species 1 and 2).

T / º C	T908 / wt%	τ_1 / ns	τ_2 / ns	ϕ_1	ϕ_2
25	0	11 ± 1	152 ± 3	1.6	98.4
	0.2	3.09 ± 0.07	115 ± 2	15.9	84.1
	0.4	0.6 ± 0.1	103 ± 3	39.7	60.3
	0.5	0.7 ± 0.1	101 ± 3	45.9	54.1
	0.7	0.90 ± 0.08	92 ± 3	57.2	42.8
50	0	4.8 ± 0.3	117 ± 1	3.0	97.0
	0.2	3.76 ± 0.05	47.9 ± 0.8	57.5	42.5
	0.4	4.49 ± 0.06	34.5 ± 0.7	72.6	27.4
	0.5	3.85 ± 0.05	26.7 ± 0.6	79.1	20.9
	0.7	3.33 ± 0.07	22.2 ± 0.5	78.1	21.9

ϕ_x represents the relative fluorescence intensity of each species (pyrene and impurities), calculated as

$$\phi_x = \frac{B_x\tau_x}{B_x\tau_x + B_y\tau_y} \times 100$$

At both temperatures studied, the lifetime of pyrene, τ_2, diminishes with T908 concentration, as expected, and the temperature induces a faster fall in the lifetime at the same concentration. Stern-Volmer constants for the quenching with T908 at both temperatures were obtained by using Eq. 7. In order to ensure unimers were the only species in solution, only data below the *cmc* (0.16 mM) were used, resulting in 3.5 ± 0.5 M^{-1} at 25 ºC ($K_{D,25ºC}$) and 17.90 ± 0.08 M^{-1} at 50 ºC ($K_{D,50ºC}$). The fact that $K_{D,25ºC} < K_{D,50ºC}$ indicates a typical dynamic quenching process. The rate of collisions increases with temperature, producing a reduction in the relative fluorescence intensity of pyrene. Interestingly, no quenching was observed between pyrene and 4000-PEG (SI, Figure 4), suggesting that it is the PPO moiety, containing the diamine spacer, which is responsible for the attenuation of the fluorescence. The Stern-Volmer constant obtained with concentrations above the *cmc* at 50 ºC resulted in $K_{D,50ºC}$ = 15 ± 1 M^{-1}, which is close to that obtained over the unimers concentration range at that temperature.

Concentrated regime: The Gel Phase. Raising the temperature and/or increasing the concentration of T908 induces the formation of physical gels (Figure 1). Firstly, the interval up to 15% was studied before focusing on the gel phase at higher concentration. In this region, a mixture of both unimers and micelles in solution is expected, depending on the temperature and concentration. As an example, SANS curves for 10% T908 are shown in Figure 5. At 20 ºC, there are no micelles in solution, which is reflected by the low scattering and a shape of the curve similar to the one at 1% (Figure 3A). At 30 ºC, a small fraction of micelles is present; from 40 ºC, and more so at 50 ºC, the fraction of micelles increases. Focusing on the scattering at 50ºC, in spite of the higher fraction of micelles, the presence of unimers is not negligible and must be taken into account (since the cmc is 0.4 % at this temperature). In addition, there will be a certain excess scattering in the high q-region, due to the dissolved chains of PEO surrounding the core, which become visible at high concentrations[39]. To include all these contributions, we have built a fitting model that accounts for the interactions between core-shell spheres with a HS structure factor, and incorporates the scattering due to the free unimers plus the chains of PEO surrounding the core into an empirical Lorentz-type function, with an associated correlation length ξ, which gives an estimate of the average entanglement length for a semi-dilute solution of polymeric chains. The results obtained with this model for a 10% Tetronic solution are shown in Table 1. For the micelles, ρ_{core} was left to float, resulting in a considerably higher value than that of pure PPO ($\rho_{core} = 4.02 \cdot 10^{-6}$ Å^{-2}), which reflects that, apart from the shell, the micellar core is also considerably hydrated, with n_{solv}/PO = 44. Micellar sizes of around 9 nm in radius were obtained, slightly smaller and with a lower N_{agg} than in the dilute regime (N_{agg} = 13), as a result of the increased core hydration and smaller shell thickness. Regarding the effect of pH at intermediate concentrations of poloxamine, it is similar to that observed in dilute conditions, namely, micellization is inhibited at acidic pH, even at 50 ºC (Figure 5).

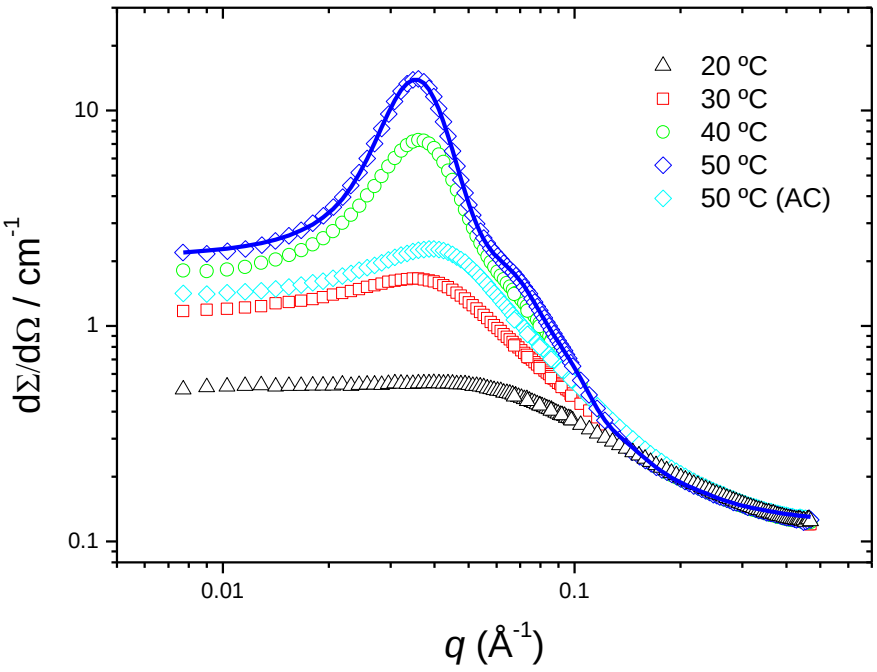

Figure 5. SANS curves for 10% T908 in D_2O as a function of temperature at natural and acidic (AC) pH. The solid line is the fit to a CSS-HS + four-arm star polymer.

The aggregation of T908 at 10% was further studied by FTIR. Infrared spectroscopy provides information at a molecular level on changes in the chemical surroundings of specific functional groups, such as those occurring during the micellization. The aggregation of Pluronic F127[47] and Tetronic T1107[22] were recently studied by this technique by monitoring the band at 1085 cm^{-1}, which corresponds to the combination of stretching and vibration bands of the C-O-C from EO and PO monomers. The results obtained for T908 as a function of the temperature are shown in SI, Figure 5. In this plot, the maximum wavenumber at 20 ºC (1082.75 cm^{-1}) was subtracted from the value at each temperature (SI, Figure 5A), showing a small but significant shift of the C-O-C band to higher wavenumbers. This shift is more gradual (from 30 to 50 ºC) in T908 than the observed with T1107 which, at the same time, is smoother than that for Pluronic F127. The more open structure of T908 (large hydrophilic chain), capable of accommodating a large number of solvent molecules compared to T1107 may explain why changes in hydration occur smoothly.

Increasing the concentration of T908 induces the formation of physical gels (see the phase diagram in D_2O in Figure 1). Figure 6 shows the SANS patterns obtained with

30% T908 at non-buffered pH (ca 8.8) as a function of the temperature. At 25 ºC, both unimers and micelles coexist. Only a combined model with star polymer, CSS and HS (due to high the concentrations used) would be required to provide a satisfactory fit. Raising the temperature induces the full aggregation into micelles and their organization into a macro-lattice structure, leading to gel formation.

The long-range order sustaining the gel is visible from the sharp diffraction peaks in the 0.07-0.09 $Å^{-1}$ *q*-region, typical of a paracrystalline structure. We fitted the data with the three cubic models: SCC (simple cubic), FCC (face centred), and BCC (body centred), and the best fits were obtained with the latter type of packing, in accordance with Habas et al.[31] for this block copolymer. In these models, the radius of the sphere corresponds roughly to the micellar core plus the denser part of the corona, as the shell is formed by largely hydrated PEO, with a low contrast compared to the solvent. According to this, the sld of the spheres was set to that of PPO ($\rho_{PO} = 3.44 \cdot 10^{-7}$ $Å^{-2}$), which corresponds to the core of the micelle. The lattice spacing (*dnn*) and volume fraction of the spheres (ϕ) were set as floating parameters. The different calculated parameters at natural and intermediate pHs are shown in Table 3.

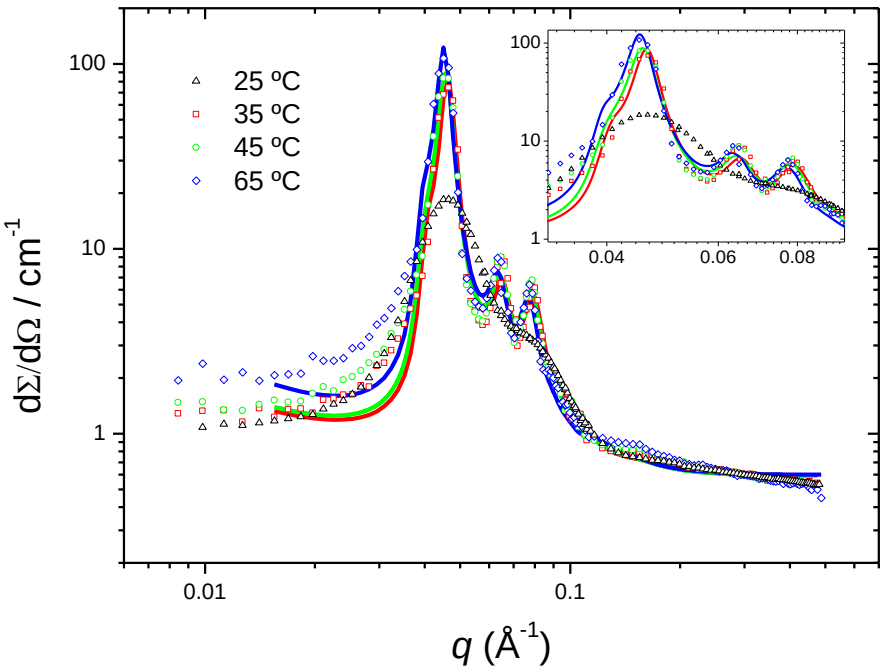

Figure 6. SANS curves for 30% T908 in D_2O as a function of temperature at natural pH. Solid lines are fits to the different models as described in the text.

The radius of the packed spheres is 30, 31 and 35 Å at 35, 45 and 65 ºC, respectively, in excellent agreement with the micellar core size in dilute conditions (R_c = 31.6 Å). The micellar volume fractions are close to 0.68 (Table 3) as expected for a BCC packing. At 35 and 45 ºC, the volume fractions obtained are higher than 0.68, which suggest a certain degree of overlap of the hydrophilic shells from neighboring micelles. Assuming an ideal BCC packing, where spheres are in contact along the diagonal of the cube, the radius of the micelle (R) is given by

$$R = \frac{\sqrt{3}}{4} dnn \qquad \text{Eq. 8}$$

resulting sizes of 83, 84 and 85 Å, at 35, 45 and 65 ºC respectively. These values are somewhat lower than those obtained under dilute conditions (R = 10 nm, Table 1), most likely because of the overlapping of the shells in the concentrated regime. A similar size was reported by Habas et al., who obtained 78 Å as the total micellar radius for 30% T908 at 38 ºC.[31]

Table 3. Structural parameters of 30% T908 extracted from SANS data analysis: *d factor* (paracrystal distortion factor), *dnn* (lattice spacing), ϕ (volume fraction of spheres), R_c (sphere radius), R (total micellar radius).

T / ºC	pH	*d* factor	*dnn* / Å	ϕ	R_c / Å	$R_{micelle}$ / Å
35	8.8	0.0784	192	0.75	30	83
45	8.8	0.0776	194	0.74	31	84
65	8.8	0.0790	196	0.63	35	85
45	6.6	0.0803	191	0.71	30	83
65	6.6	0.0796	196	0.64	34	85

The effect of pH was studied for a 30% T908 solution (Figure 7A). At pH = 6.6, higher temperatures (ca. 10ºC higher) are required to achieve the gelation of the system compared to natural pH. The nanostructural features are similar to those obtained at natural pH (Table 3), meaning that intermediate pH shifts the onset of gelation but does not affect micellar shape and packing.

As expected, acidic pH (pH = 1.6) totally inhibits the formation of a paracrystalline structure, which is reflected in the SANS patterns as the absence of sharp diffraction peaks and a lower overall scattering (Figure 7B). In those conditions, small micelles (with radius of 62 and 67 Å, at 45 and 65 ºC, respectively) with low aggregation numbers (< 4) are obtained from the CSS-HS model (data not shown), showing

further hindrance to micellization at very acidic pH, compared to natural and intermediate pHs.

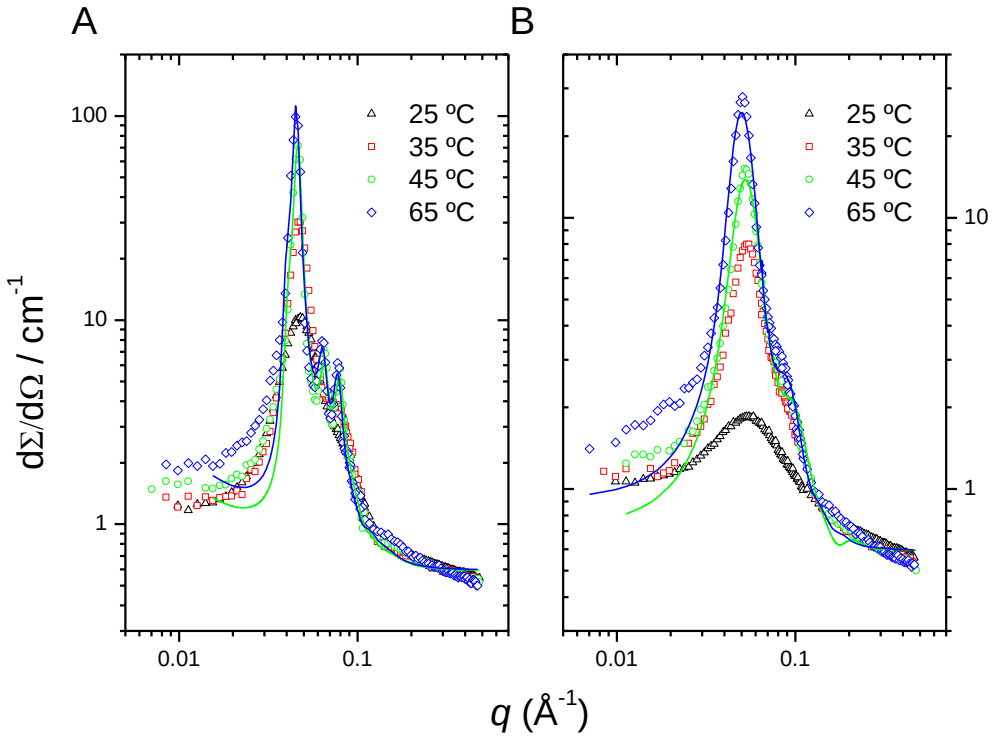

Figure 7. SANS curves for 30% T908 in D_2O as a function of temperature: (A) at pH = 6.6; and (B) at pH = 1.6. Solid lines are fits to the different models.

Overall, the SANS measurements in the concentrated regime demonstrate the influence of temperature, concentration and pH on structure and the gelation process.

Next, oscillatory rheology is used to study the mechanical properties of the gels, by following the evolution of the elastic (*G'*) and viscous (*G''*) modulus as a function of temperature and frequency. Figure 8 shows temperature curves measured over the range 20 to 80°C at natural pH, fixed strain (1%) and frequency (6.28 rad·s^{-1}). All curves show a smooth increase of both moduli as the temperature increases, reflecting an increase in both the elasticity and the viscosity of the solutions. From 20% T908, both moduli reach a plateau, preceded by a sharp increase, which shifts to lower temperatures as the concentration increases. From the phase behaviour studies, using the crude method of tube inversion, no gel was detected at 10% and 15%, which here is denoted by the absence of a plateau in the temperature sweep. At higher concentrations, the plateau is reached at 55, 42 and 35 ºC for 20, 25 and 30 % of T908, respectively, in agreement with the phase diagrams (Figure 1) and SANS results

(Figure 6), in which the sharp crystalline peaks denoting the appearance of a macrolattice obtained at 35 ºC with 30% of T908. At 20%, a decrease of both moduli is detected at ca. 70 ºC, which however does not lead to flow (Figure 1). Gels with higher elastic modulus (*G'*) are obtained for 25 and 30% of T908 (ca. 30k Pa). Several criteria are used in the literature to determine the temperature of gelation (T_{gel}), such as the cross-over between *G'* and *G''*, or an arbitrary threshold value of *G'*.[48,49] Here it is clear from the phase diagrams that the very high values reached by *G'* and *G''*, or indeed the predominance of *G'* and G'', do not reflect the onset of a gel phase, and a full frequency sweep at these temperatures would probably show a predominantly solid-like behaviour at high frequencies with however a liquid-like behaviour (flow) occurring over a substantial range of frequencies, since these samples were shown to flow in the tube inversion test. Instead, the onset of gelation seem to correspond to the appearance of the plateau, and a frequency sweep of 30% T908 at 50 ºC (SI, Figure 6) indeed shows *G'* higher than *G''* over a wide range of frequencies, denoting a highly structured sample, with very large relaxation times. *G'* and *G''* are however both dependent on frequency, showing a behaviour similar to entanglement networks, rather than crosslinked gels.

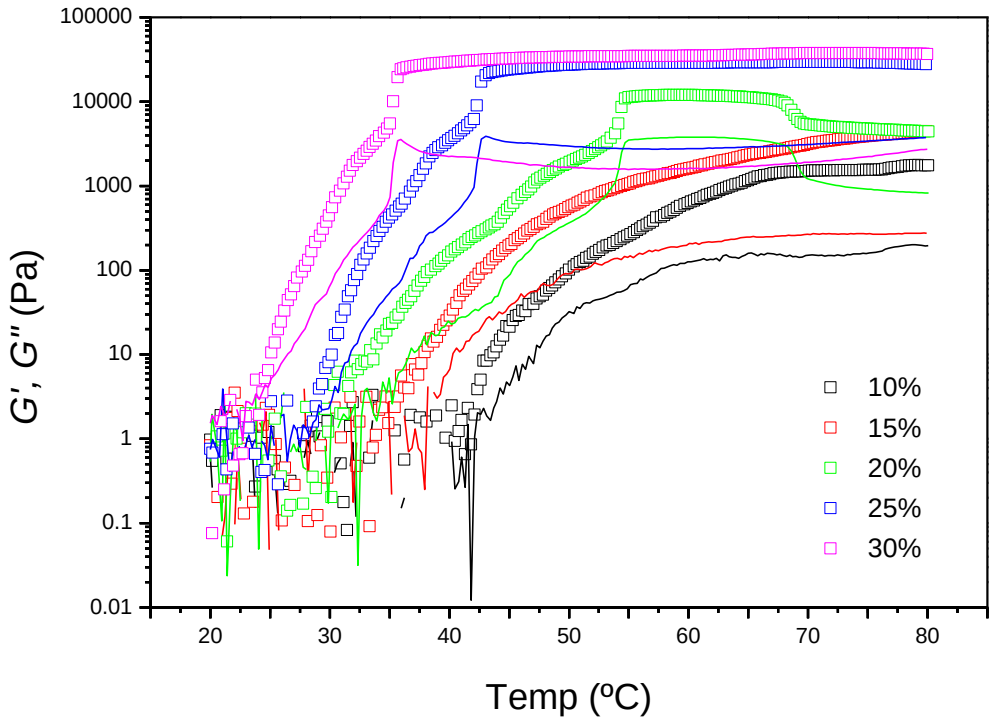

Figure 8. Oscillatory rheology data (□ *G'* and – *G"*) showing temperature sweeps as a function of T908 concentration in water at natural pH, 6.28 rad·s^{-1} frequency, 1% strain and 2 ºC/min heating rate.

At intermediate pH (Figure 9), the gels are obtained at 40 and 55 ºC for 30 and 25%, respectively. For 20% T908, gelation does not occur, a behaviour similar to the one observed at 15% at natural pH, while gel phase is obtained for 25 and 30% over a wide range of temperatures. For 30% of T908, the results are in accordance with SANS data, where the well-defined paracrystalline structure of the gels was obtained at 45 ºC, but not at 35 ºC (Figure 7A).

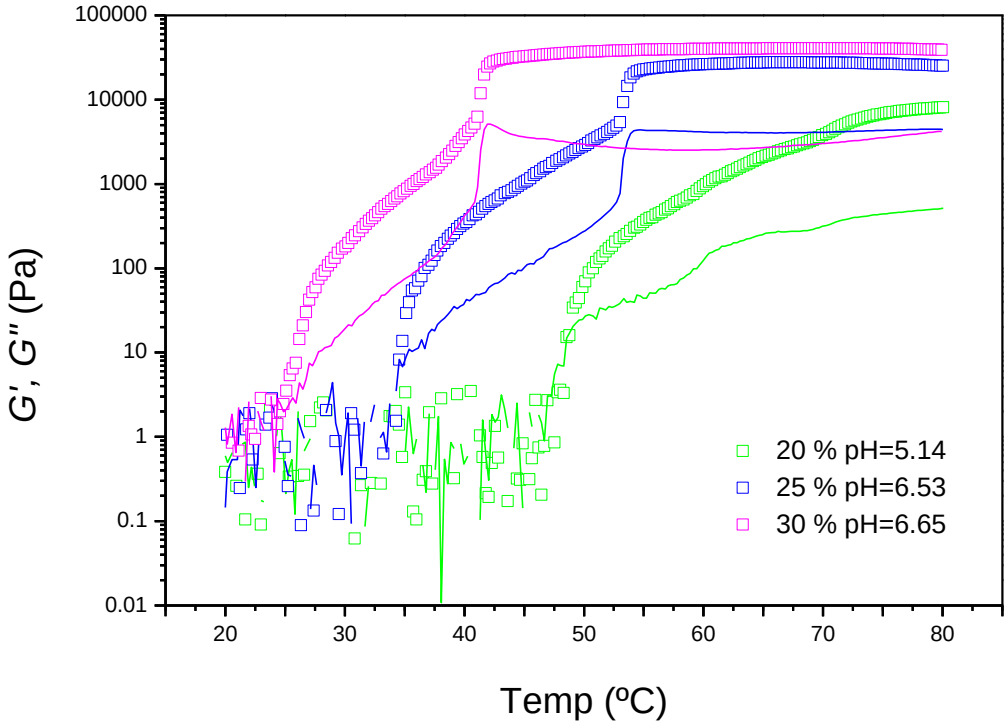

Figure 9. Oscillatory rheology data (□ *G'* and – *G"*) showing temperature sweeps as a function of the T908 concentration in water at intermediate pH, 6.28 rad·s^{-1} frequency, 1% strain and 2 ºC/min heating rate.

Figure 10 summarizes the effect of pH by comparing the traces of *G'* obtained at natural and intermediate pHs. The figure clearly shows the shift in the gelation temperature as the pH decreases. This effect is more pronounced at lower temperatures. However, for both pH conditions, the same general behavior is observed, with this shift in T_{gel}.

Overall, higher temperatures are required at intermediate pH to achieve the gelation of the systems. However, once a threshold concentration and temperature are reached, similar *G'* values are obtained to those at natural pH, in line with the similar structural features of the gels deduced from SANS.

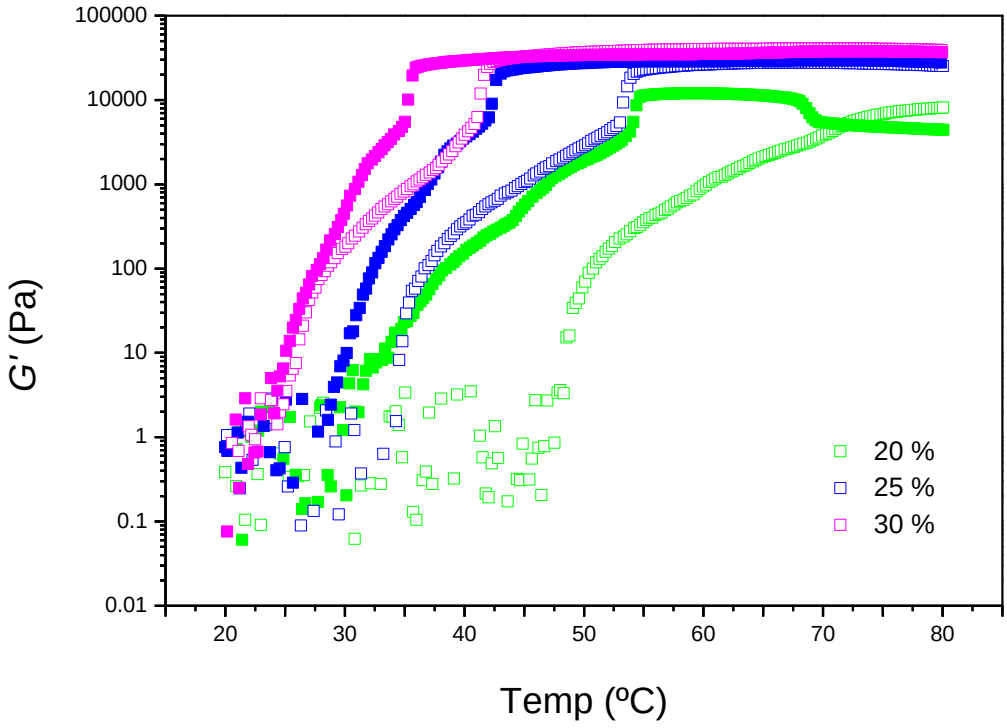

Figure 10. Oscillatory rheology data (■ natural and □ intermediate pHs) showing temperature sweeps as a function of the T908 concentration in water, 6.28 rad·s^{-1} frequency, 1% strain and 2 ºC/min heating rate.

Finally, the effect of replacing water by D_2O as the solvent on the gel behavior was examined. SI, Figure 7 clearly shows the shift in the onset of gelation towards lower temperatures in D_2O, compared to H_2O, as already identified by visual observation (Figure 1, SI, Figure 1 and SI, Figure 2), in accordance with Gille et al.[38] and the different relative strength of the hydrogen bond network, as explained above.

CONCLUSIONS

This work reports the micellization and gelation process of a very large, highly hydrophilic tetrablock copolymer: Tetronic 908 (T908), as a function of temperature, concentration and pH. A minimum temperature is required for the formation of micelles at low concentration of the amphiphile. Those micelles display a core-shell

architecture with a dehydrated core and a highly hydrated shell (94% D_2O), with relatively small aggregation numbers (Nagg = 13 at 1% and 50 ºC), lower than other less hydrophilic poloxamines. Micellization is notably affected by the degree of protonation of the central amine spacer, producing a shift of the *cmc* to higher concentration at acidic pH. In the concentrated regime, the micellised fraction increases and strong inter-micellar interactions are detected. At 10 and 15 %, the micelles are slightly smaller and present a higher hydration of the core than in the dilute regime. At high concentration (> 20%) and temperature, T908 undergoes a sol-to-gel transition. SANS data analysis shows the onset of long-range order reflected by sharp scattering peaks, which are consistent with a BCC order of tightly packed spheres. This compact packing of the micelles results in a slight shrinkage of the micelles, compared to dilute conditions, implying some overlapping of the PEO-containing shells. The temperature of gelation decreases as the concentration increases, and the value of the elastic modulus, *G'*, also increases. The pH hinders the gelation process: at intermediate pH, between pKa_1 and pKa_2, the gelation is shifted to higher temperatures, however, once gels are formed, the morphology of the gels is identical to natural pH. At very acidic pH, the gelation is completely suppressed.

Overall, the morphology of the micelles and gel characteristics of T908 are very close to Pluronic F127, which has been widely used as a drug nanocarrier, in particular in the cancer arena, because of its ability to overcome multidrug resistance. This makes T908 an equally, or perhaps superior, candidate, because of the added feature of pH-responsiveness, which provides an additional handle towards targeted delivery. Given the already proven potential of T908 as a biomaterial, this study provides a strong structural basis towards the development of T908 micellar gels for bespoke delivery applications.

ACKNOWLEDGMENTS

The authors are grateful to JCNS at the Heinz Maier-Leibnitz Zentrum (MLZ), Garching, Germany, for financial support and beam-time and to G. Mangiapia for his assistance with the SANS experiments and data reduction. Financial support from project MAT2014-59116-C2-2-R of the Spanish MINECO and the Asociación de Amigos de la Universidad de Navarra for the doctoral grant of J.P. is acknowledged.

REFERENCES

(1) Alexandridis, P. Poly(ethylene Oxide)/poly(propylene Oxide) Block Copolymer Surfactants. *Curr. Opin. Colloid Interface Sci.* **1997**, *2* (5), 478–489.

(2) Alakhova, D. Y.; Kabanov, A. V. Pluronics and MDR Reversal: An Update. *Mol. Pharm.* **2014**, *11* (8), 2566–2578.

(3) Mortensen, K.; Pedersen, J. S. Structural Study On The Micelle Formation of Poly(Ethylene Oxide)-Poly(Propylene Oxide)-Poly(Ethylene Oxide) Triblock CopolymerE in Aqueous-Solution. *Macromolecules* **1993**, *26* (4), 805–812.

(4) Svensson, B.; Olsson, U.; Alexandridis, P.; Mortensen, K. A SANS Investigation of Reverse (Water-in-Oil) Micelles of Amphiphilic Block Copolymers. *Macromolecules* **1999**, *32* (20), 6725–6733.

(5) Ma, J. H.; Guo, C.; Tang, Y. L.; Liu, H. Z. H-1 NMR Spectroscopic Investigations on the Micellization and Gelation of PEO-PPO-PEO Block Copolymers in Aqueous Solutions. *Langmuir* **2007**, *23* (19), 9596–9605.

(6) Kabanov, A. V.; Batrakova, E. V.; Miller, D. W. Pluronic (R) Block Copolymers as Modulators of Drug Efflux Tranporter Activity in the Blood-Brain Barrier. *Adv. Drug Deliv. Rev.* **2003**, *55* (1), 151–164.

(7) Batrakova, E. V.; Kabanov, A. V. Pluronic Block Copolymers: Evolution of Drug Delivery Concept from Inert Nanocarriers to Biological Response Modifiers. *J. Control. Release* **2008**, *130* (2), 98–106.

(8) Kabanov, A. V.; Alakhov, V. Y. Pluronic Block Copolymers in Drug Delivery: From Micellar Nanocontainers to Biological Response Modifiers. *Crit. Rev. Ther. Drug Carrier Syst.* **2002**, *19* (1), 1–72.

(9) Alexandridis, P.; Alan Hatton, T. Poly(ethylene Oxide)-Poly(propylene Oxide)-Poly(ethylene Oxide) Block Copolymer Surfactants in Aqueous Solutions and at Interfaces: Thermodynamics, Structure, Dynamics, and Modeling. *Colloids Surfaces A Physicochem. Eng. Asp.* **1995**, *96* (1–2), 1–46.

(10) Schmolka, I. R. A Review of Block Polymer Surfactants. *J. Am. Oil Chem. Soc.* **1977**, *54* (3), 110–116.

(11) Schmolka, I. R. Gel Cosmetics. *Cosmet. Toilet.* **1984**, *99* (11), 69.

(12) Raval, A.; Pillai, S. A.; Bahadur, A.; Bahadur, P. Systematic Characterization of Pluronic ® Micelles and Their Application for Solubilization and in Vitro Release of Some Hydrophobic Anticancer Drugs. *J. Mol. Liq.* **2017**, *230*, 473–481.

(13) Nishiyama, N.; Kataoka, K. Current State, Achievements, and Future Prospects of Polymeric Micelles as Nanocarriers for Drug and Gene Delivery. *Pharmacol. Ther.* **2006**, *112* (3), 630–648.

(14) Valero, M.; Dreiss, C. A. Growth, Shrinking, and Breaking of Pluronic Micelles in the Presence of Drugs And/or β-Cyclodextrin, a Study by Small-Angle Neutron Scattering and Fluorescence Spectroscopy. *Langmuir* **2010**, *26* (13), 10561–10571.

(15) Alexandridis, P.; Spontak, R. J. Solvent-Regulated Ordering in Block Copolymers. *Curr. Opin. Colloid Interface Sci.* **1999**, *4* (2), 130–139.

(16) Pispas, S.; Poulos, Y.; Hadjichristidis, N. Micellization Behavior of (PS)(8)(PI)(8) Miktoarm (Vergina) Star Copolymers. *Macromolecules* **1998**, *31* (13), 4177–4181.

(17) Egan, R. W.; Jones, M. A.; Lehninger, A. L. Hydrophile-Lipophile Balance and Critical Micelle Concentration as Key Factors Influencing Surfactant Disruption of Mitochondrial-Membranes. *J. Biol. Chem.* **1976**, *251* (14), 4442–4447.

(18) Gonzalez-Lopez, J.; Alvarez-Lorenzo, C.; Taboada, P.; Sosnik, A.; Sandez-Macho, I.; Concheiro, A. Self-Associative Behavior and Drug-Solubilizing Ability of Poloxamine (Tetronic) Block Copolymers. *Langmuir* **2008**, *24* (19), 10688–10697.

(19) Larrañeta, E.; Isasi, J. R. Phase Behavior of Reverse Poloxamers and Poloxamines in Water. *Langmuir* **2013**, *29* (4), 1045–1053.

(20) Sosnik, A.; Sefton, M. V. Methylation of Poloxamine for Enhanced Cell Adhesion. *Biomacromolecules* **2006**, *7* (1), 331–338.

(21) González-Gaitano, G.; da Silva, M. A.; Radulescu, A.; Dreiss, C. A. Selective Tuning of the Self-Assembly and Gelation of a Hydrophilic Poloxamine by Cyclodextrins. *Langmuir* **2015**, *31* (20), 5645–5655.

(22) Serra-Gomez, R.; Dreiss, C. A.; Gonzalez-Benito, J.; Gonzalez-Gaitano, G. Structure and Rheology of Poloxamine T1107 and Its Nanocomposite Hydrogels with Cyclodextrin-Modified Barium Titanate Nanoparticles. *Langmuir* **2016**, *32* (25), 6398–6408.

(23) Gonzalez-Gaitano, G.; Muller, C.; Radulescu, A.; Dreiss, C. A. Modulating the Self-Assembly of Amphiphilic X-Shaped Block Copolymers with Cyclodextrins: Structure and Mechanisms. *Langmuir* **2015**, *31* (14), 4096–4105.

(24) Bahadur, A.; Cabana-Montenegro, S.; Aswal, V. K.; Lage, E. V.; Sandez-Macho, I.; Concheiro, A.; Alvarez-Lorenzo, C.; Bahadur, P. NaCl-Triggered Self-Assembly of Hydrophilic Poloxamine Block Copolymers. *Int. J. Pharm.* **2015**, *494* (1), 453–462.

(25) Simoes, S. M. N.; Veiga, F.; Torres-Labandeira, J. J.; Ribeiro, A. C. F.; Concheiro, A.; Alvarez-Lorenzo, C. Poloxamine-Cyclodextrin-Simvastatin Supramolecular Systems Promote Osteoblast Differentiation of Mesenchymal Stem Cells. *Macromol. Biosci.* **2013**, *13* (6), 723–734.

(26) Puga, A. M.; Rey-Rico, A.; Magariños, B.; Alvarez-Lorenzo, C.; Concheiro, A. Hot Melt Poly-ε-Caprolactone/poloxamine Implantable Matrices for Sustained Delivery of Ciprofloxacin. *Acta Biomater.* **2012**, *8* (4), 1507–1518.

(27) Moghimi, S. M.; Muir, I. S.; Illum, L.; Davis, S. S.; Kolb-Bachofen, V. Coating Particles with a Block Co-Polymer (Poloxamine-908) Suppresses Opsonization but Permits the Activity of Dysopsonins in the Serum. *Biochim. Biophys. Acta - Mol. Cell Res.* **1993**, *1179* (2), 157–165.

(28) Redhead, H. M.; Davis, S. S.; Illum, L. Drug Delivery in Poly(lactide-Co-Glycolide) Nanoparticles Surface Modified with Poloxamer 407 and Poloxamine 908: In Vitro Characterisation and in Vivo Evaluation. *J. Control. Release* **2001**, *70* (3), 353–363.

(29) Perreur, C.; Habas, J. P.; François, J.; Peyrelasse, J.; Lapp, A. Determination of the Structure of the Organized Phase of the Block Copolymer PEO-PPO-PEO in Aqueous Solutions under Flow by Small-Angle Neutron Scattering. *Phys. Rev. E* **2002**, *65* (4), 41802.

(30) Branca, C.; Magazu, S.; Migliardo, F. Star Polymer/water Solutions: New Experimental Findings. *Condens. Matter Phys.* **2002**, *5*, 275–284.

(31) Habas, J.-P.; Pavie, E.; Perreur, C.; Lapp, A.; Peyrelasse, J. Nanostructure in Block Copolymer Solutions: Rheology and Small-Angle Neutron Scattering. *Phys. Rev. E* **2004**, *70* (61802), 1–8.

(32) Hamley, I. W.; Daniel, C.; Mingvanish, W.; Mai, S. M.; Booth, C.; Messe, L.; Ryan, A. J. From Hard Spheres to Soft Spheres: The Effect of Copolymer Composition on the Structure of Micellar Cubic Phases Formed by Diblock Copolymers in Aqueous Solution. *Langmuir* **2000**, *16* (6), 2508–2514.

(33) Odhner, H.; Jacobs, D. T. Refractive Index of Liquid D_2O for Visible Wavelengths. *J. Chem. Eng. Data* **2012**, *57* (1), 166–168.

(34) Cho, C. H.; Urquidi, J.; Singh, S.; Robinson, G. W. Thermal Offset Viscosities of Liquid H2O, D2O, and T2O. *J. Phys. Chem. B* **1999**, *103* (11), 1991–1994.

(35) Radulescu, A.; Szekely, N. K.; Appavou, M.-S.; Pipich, V.; Kohnke, T.; Ossovyi, V.; Staringer, S.; Schneider, G. J.; Amann, M.; Zhang-Haagen, B.; et al. Studying Soft-Matter and Biological Systems over a Wide Length-Scale from Nanometer and Micrometer Sizes at the Small-Angle Neutron Diffractometer KWS-2. *J. Vis. Exp.* **2016**, No. 118, e54639.

(36) Http://www.sasview.org/. Developed by the DANSE Project under NSF Award DMR-0520547.

(37) Benoit, H. On the Effect of Branching and Polydispersity on the Angular Distribution of the Light Scattered by Gaussian Coils. *J. Polym. Sci.* **1953**, *11* (5), 507–510.

(38) Gille, K.; Knoll, H.; Rittig, F.; Fleischer, G.; Kärger, J. Study of Structure Formation in Aqueous Solutions of Poly(ethylene oxide)−Poly(propylene oxide)−Poly(ethylene Oxide) Block Copolymers by Measuring Rate Constants of the Thermal Cis−Trans Isomerization of an Azobenzene Dye and Self-Diffusion of Copolymer M. *Langmuir* **1999**, *15* (4), 1059–1066.

(39) Valero, M.; Castiglione, F.; Mele, A.; da Silva, M. A.; Grillo, I.; González-Gaitano, G.; Dreiss, C. A. Competitive and Synergistic Interactions between Polymer Micelles, Drugs, and Cyclodextrins: The Importance of Drug Solubilization Locus. *Langmuir* **2016**, *32* (49), 13174–13186.

(40) Hammouda, B. SANS from Pluronic P85 in D-Water. *Eur. Polym. J.* **2010**, *46* (12), 2275–2281.

(41) Kalyanasundaram, K.; Thomas, J. K. Environmental Effects on Vibronic Band Intensities in Pyrene Monomer Fluorescence and Their Application in Studies of Micellar Systems. *J. Am. Chem. Soc.* **1977**, *99* (7), 2039–2044.

(42) Ananthapadmanabhan, K. P.; Goddard, E. D.; Turro, N. J.; Kuo, P. L. Fluorescence Probes for Critical Micelle Concentration. *Langmuir* **1985**, *1*, 352–355.

(43) Aguiar, J.; Carpena, P.; Molina-Bolívar, J. A.; Ruiz, C. C. On the Determination of the Critical Micelle Concentration by the Pyrene 1:3 Ratio Method. *J. Colloid Interface Sci.* **2003**, *258*, 116–122.

(44) Ribeiro, A.; Sosnik, A.; Chiappetta, D. A.; Veiga, F.; Concheiro, A.; Alvarez-Lorenzo, C. Single and Mixed Poloxamine Micelles as Nanocarriers for

Solubilization and Sustained Release of Ethoxzolamide for Topical Glaucoma Therapy. *J. R. Soc. Interface* **2012**, *9* (74), 2059–2069.

(45) Geiger, M. W.; Turro, N. J. Pyrene Fluorescence Lifetime As A Probe For Oxygen Penetration Of Micelles. *Photochem. Photobiol.* **1975**, *22* (6), 273–276.

(46) Piñeiro, L.; Novo, M.; Al-Soufi, W. Fluorescence Emission of Pyrene in Surfactant Solutions. *Adv. Colloid Interface Sci.* **2015**, 1–12.

(47) Su, Y. L.; Wang, J.; Liu, H. Z. FTIR Spectroscopic Investigation of Effects of Temperature and Concentration on PEO−PPO−PEO Block Copolymer Properties in Aqueous Solutions. *Macromolecules* **2002**, *35* (16), 6426–6431.

(48) Bode, F.; da Silva, M. A.; Drake, A. F.; Ross-Murphy, S. B.; Dreiss, C. A. Enzymatically Cross-Linked Tilapia Gelatin Hydrogels: Physical, Chemical, and Hybrid Networks. *Biomacromolecules* **2011**, *12* (10), 3741–3752.

(49) da Silva, M. A.; Farhat, I. A.; Areas, E. P. G.; Mitchell, J. R. Solvent-Induced Lysozyme Gels: Effects of System Composition and Temperature on Structural and Dynamic Characteristics. *Biopolymers* **2006**, *83* (5), 443–454.

Electronic Supplementary Material

Click here to download 7: Electronic Supplementary Material: Supporting information T908.docx